Systematic reduction of the proton-removal cross section in neutron-rich medium-mass nuclei

J. Díaz-Cortés [a], J. Benlliure [a,*], J.L. Rodríguez-Sánchez [a], H. Álvarez-Pol [a], T. Aumann [b],
C.A. Bertulani [c], B. Blank [d], E. Casarejos [e], D. Cortina-Gil [a], D. Dragosavac [a], V. Föhr [f],
A. Gargano [g], M. Gascón [a], W. Gawlikowicz [h], A. Heinz [j], K. Helariutta [k], A. Kelić-Heil [f],
S. Lukić [f], F. Montes [f,1], D. Pérez-Loureiro [a,2], L. Pieńkowski [i], K.-H. Schmidt [f], M. Staniou [f],
K. Subotić [l], K. Sümmerer [f], J. Taieb [m], A. Trzcińska [i]

[a] IGFAE, Universidade de Santiago de Compostela, E-15782, Spain
[b] Institut für Kernphysik, Technische Universität Darmstadt, 64289 Darmstadt, Germany
[c] Texas A&M University-Commerce, 75428 Commerce, TX, United States of America
[d] Centre d'Etudes Nucleaires, F-33175 Bordeaux-Gradignan Cedex, France
[e] University of Vigo, E-36200 Vigo, Spain
[f] GSI Helmholtzzentrum für Schwerionenforschung, D-64291 Darmstadt, Germany
[g] Istituto Nazionale di Fisica Nucleare, Complesso Universitario di Monte S. Angelo, Via Cintia, I-80126 Napoli, Italy
[h] Cardinal Stefan Wyszynski University, PL-01-938 Warsaw, Poland
[i] Heavy Ion Laboratory, University of Warsaw, PL-02-093 Warsaw, Poland
[j] Chalmers University of Technology, SE-41296 Gothenburg, Sweden
[k] University of Helsinki, FI-00014 Helsinki, Finland
[l] Institute of Nuclear Sciences Vinča, University of Belgrade, 11001 Belgrade, Serbia
[m] CEA, DAM, DIF, F-91297 Arpajon, France

ARTICLE INFO

ABSTRACT

Single-neutron and single-proton removal cross sections have been measured for medium-mass neutron-rich nuclei around $Z = 50$ and energies around $1000A$ MeV using the FRagment Separator (FRS) at GSI. The measured cross sections confirm the relative low values of the proton-removal cross sections, observed since a long time ago and not yet understood. Model calculations considering the knock-out process together with initial- and final-state interactions describe the measured neutron-removal cross sections. Proton-removal cross sections are, however, significantly over-predicted by the same calculations. The observed difference can be explained to a large extent by the knock-out of short-range correlated nucleons from dominant neutron-proton pairs in neutron-rich nuclei.

© 2020 The Author(s). Published by Elsevier B.V. This is an open access article under the CC BY license (http://creativecommons.org/licenses/by/4.0/). Funded by SCOAP³.

1. Introduction

Single-nucleon knock-out reactions at intermediate and high energies are a widely-used tool to investigate the structure of the atomic nucleus, as the removed nucleon is expected to provide information on the previously occupied single-particle state. The success of knock-out studies is due not only to the well-defined experimental conditions characterizing these reactions, but

also to the relatively simple theoretical description provided by Eikonal models. Following these ideas, direct kinematics $(e, e'p)$ low-momentum transfer experiments on stable nuclei, performed in the 80s and 90s, probed the limits of the independent particle shell-model picture. Those investigations showed a 30-40% reduction in the spectroscopic factors quantifying the shell-model fragmentation of the occupancy of single-particle states around the Fermi level [1,2]. Less than half of this reduction has been attributed to long-range correlations responsible for collective nuclear modes [3,4]. Similar investigations, using proton beams, have provided complementary information on the single-particle structure of stable nuclei [5].

High momentum-transfer proton knock-out experiments induced by electrons [6] and protons [7] probed the existence of short-lived correlated nucleon pairs by the identification of knock-

out nucleons forming pairs with relatively low center-of-mass momentum ($k_{tot} < k_F$) but rather large relative momentum ($k_{rel} > k_F$). Those short-range correlated (SRC) nucleon pairs, produced by the short-range components (scalar or tensor) of the nuclear force, involve around 20% of the nucleons in a given nucleus [8,9], explaining the depopulation of single-particle states below the Fermi momentum (k_F) and the population of higher energy states. Recently, it has also been shown that about 90% of the SRC pairs are neutron-proton pairs [10], indicating the dominance of the tensor interaction. As consequence, the number of protons in SRC pairs increases with neutron-excess in the nucleus [11–13].

Nucleon-induced knock-out reactions in inverse kinematics opened the possibility to study the structure of unstable fast-moving secondary projectile nuclei [14]. Moreover, exclusive single-nucleon knock-out measurements including γ-ray detection have provided spectroscopic information on the ground state of the investigated nuclei [15]. This technique has also been used more recently to explore the reduction of the single-particle spectroscopic strength around the Fermi level by introducing a "quenching" factor defined as the ratio between measured single-nucleon knock-out cross sections and calculated ones, the latter taking into account shell-model spectroscopic factors [16].

The systematic investigation of single-nucleon knock-out reactions on light projectile nuclei, covering a large range in neutron excess or separation energy, and energies up to around $100A$ MeV, not only showed a sizable quenching of the expected spectroscopic strength but also a strong dependence on the neutron excess. Indeed, it was shown that the removal of loosely bound nucleons induces a small or negligible quenching of the spectroscopic strength while the quenching for the removal of deeply bound nucleons is beyond 50% [17]. However, transfer [18] and quasi-free, $(p,2p)$ or (p,pn), nucleon removal [19,20] do not show any clear dependence of the quenching of the spectroscopic strength as function of the neutron excess for the same nuclei.

The dominance of neutron-proton SRC pairs has been proposed to contribute to the puzzling dependence of the quenching of the spectroscopic strength on the neutron excess [4]. The knock-out of a SRC proton from a neutron-rich nucleus would cause the paired nucleon, mostly a neutron, to recoil and be ejected as well [10]. Therefore, the increase of the number of SRC protons with the neutron excess [12], will reduce, accordingly, the probability of single-proton removal processes. To elucidate this discussion, and in particular the not yet explained quenching of the proton-removal cross sections in neutron-rich nuclei, we have performed a systematic investigation of single-proton and single-neutron removal reactions for medium-mass nuclei, around $Z = 50$, at relativistic energies.

2. Experiment and measurements

The experiment was performed at the GSI facility in Darmstadt, taking advantage of two different beams impinging on a 1 g/cm^2 beryllium target to produce large isotopic chains of medium-mass nuclei. Fission of $950A$ MeV ^{238}U projectiles produced neutron-rich nuclei around ^{132}Sn and fragmentation of $1200A$ MeV ^{132}Xe projectiles, leading to less neutron-rich nuclei around Z=50. As the reactions were induced in inverse kinematics at high energies, the forward-focused reaction fragments were analyzed with the FRS magnetic spectrometer [21].

In this experiment the two sections of the FRS, shown in Fig. 1, were tuned as two independent magnetic spectrometers. The first section was used to separate the medium-mass nuclei produced in the target located at the entrance of the FRS. The identification of the transmitted nuclei was achieved by measuring the magnetic rigidity (Bρ), time of flight (ToF), and energy loss (ΔE), using fast plastic scintillators located behind the first and second dipoles of
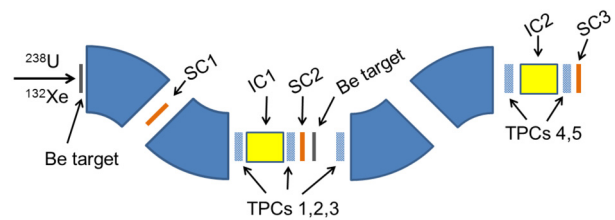

Fig. 1. Schematic representation (not to scale) of the Fragment Separator with the detection setup used in this experiment.

the FRS (SC1 and SC2), time-projection chambers (TPCs 1, 2 and 3), and a fast ionization chamber (IC1), placed at the intermediate-image plane. An additional 2591 mg/cm^2 beryllium target was placed at the intermediate-image plane to induce nucleon-removal reactions. Those reaction residues were separated using the second section of the FRS and identified by the same Bρ-ToF-ΔE method. Additional details of the experiment can be found in Ref. [28].

Fig. 2 shows the identification matrices obtained with the ^{238}U beam for a magnetic tuning of the first section of the FRS centered on ^{132}Sn (upper panel) while the setting of the second section was centered on ^{131}Sn and ^{132}In (lower panel). As can be seen, in these measurements we could not only identify the residual nuclei produced in single-nucleon removal reactions but also other residual nuclei where the projectile nucleus has lost few neutrons and protons. The resolution achieved in the isotopic identification of the fragments transmitted through the first section of the FRS was $\Delta Z/Z \approx 2.6 \ 10^{-3}$, $\Delta A/A \approx 1.2 \ 10^{-3}$, and in the second section $\Delta Z/Z \approx 3.0 \ 10^{-3}$, $\Delta A/A \approx 7.8 \ 10^{-4}$.

Cross sections were obtained normalizing the number of final fragments, identified at the final image plane of the spectrometer (lower panel in Fig. 2), to the number of incoming projectiles, identified at the intermediate image plane of the spectrometer (upper panel in Fig. 2), and the number of nuclei per surface unit of the target material. Because of some limitations of the experimental setup, the measured yields of projectile and final nuclei were corrected by loses caused by secondary reactions in all layers of matter placed at the intermediate image plane of the spectrometer, modifications in the atomic charge-state of the ions, and ion-optical transmission between the intermediate and final image planes of the spectrometer.

Although the matter at the intermediate image plane of the spectrometer caused a non negligible probability for secondary reactions, the dominance of the target in this matter load and the fact that both, projectile and final nuclei, have a similar mass number, the final corrections to the projectile and final yields were very similar and almost canceled. Indeed, this correction amounted on average to around 3% and its contribution to systematic uncertainties was estimated to be around 2%. The correction due to atomic charge states was also rather small, $\approx$2%, because of the high energies and moderate atomic number of the investigated nuclei. The contribution of this correction to the systematic uncertainty was estimated to be around 5%. The largest correction was caused by the ion-optical transmission through the spectrometer. The transmission between the intermediate and final image plane was estimated using the measured angle and momentum distributions of the incoming projectiles at the intermediate image plane of the spectrometer, and standard ion-optics model calculations. Because we run consecutive magnetic tunings of the spectrometer overlapping in magnetic rigidity, we could always select the magnetic tuning with the largest transmission for a given isotope, except for the nuclei with the largest neutron excess. Because of this reason, most of the cadmium, indium, and tin isotopes could be measured with a transmission above 90%, and only for the most neutron-rich isotopes the transmission was around 80%. For antimony and tellurium isotopes the transmission reduced on average
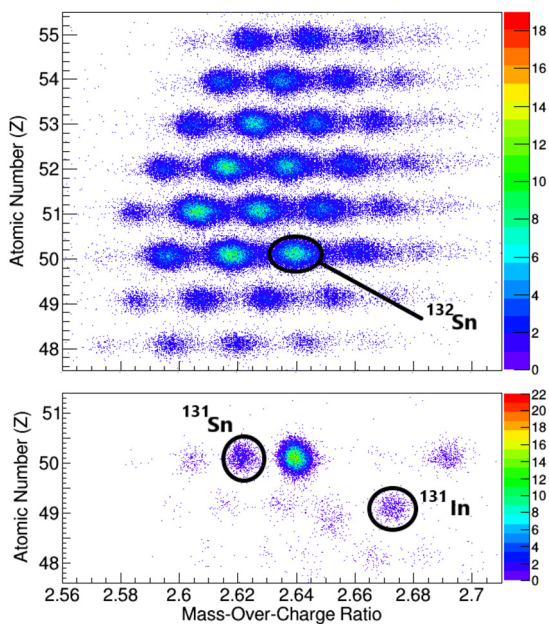
Fig. 2. Identification of the incoming cocktail beam with the first section of the FRS for a magnetic setting centered on ^{132}Sn (upper panel), and of the single-nucleon removal fragments (^{131}In and ^{131}Sn) identified with the second section of the FRS (lower panel).

down to 80% and 60%, respectively. The estimated accuracy of this correction was around 10%. Corrections associated to the thickness of the target and the data acquisition dead time were estimated to be of the order of 3% and 1%, respectively, and their contribution to the systematic uncertainty of the order of few per cent. Further details on these corrections can be found in Ref. [22].

To investigate long isotopic chains of medium-mass nuclei around $Z = 50$, several magnetic tunings of the first section of the FRS were used. Those tunings were centered on ^{119}Sn, ^{124}Sn, and ^{126}Sn for the ^{132}Xe beam, and ^{128}Sn, ^{130}Sn, ^{132}Sn, and ^{136}Sn for the ^{238}U beam. For each of these tunings, the second section of the FRS was centered on the corresponding one-neutron and one-proton removal residues. In this experiment we measured 72 single-neutron removal and 13 single-proton removal cross sections, integrated over bound excited states, although in this letter we just report the results for isotopes of tellurium, antimony, tin, and indium around $N = 82$.

Fig. 3 shows the single-neutron removal cross sections (upper panel), and the single-proton removal cross sections (lower panel), measured in this work as function of the neutron number of the initial nucleus. In both cases, the measured cross sections are rather similar for the isotones of the three elements covered by the measurements. The single-neutron removal cross sections are also similar for all isotopes from $N = 78$ until $N = 83$. At $N = 84$ all cross sections drop significantly, increasing again at $N = 85$. The observed decrease of the cross sections at $N = 84$ is explained by the fact that the excited states populated in the residual nuclei lie above the neutron separation. For $N = 84$ projectiles, the single-neutron removal produces with a large probability $N = 83$ residues with a hole state in the $1d_{3/2}$ or the $0h_{11/2}$ orbital, below the $N = 82$ shell gap, and one neutron occupying the $1f_{7/2}$ orbital above the shell gap. Those configurations correspond to excitation energies in the residual nuclei larger than the $N = 82$ gap energy, ~ 3.7 MeV. Because of these large excitation energy values, and the low neutron binding energies (S_n) of the $N = 83$ residues (e.g. $S_n(^{133}$Sn$)=2.4$ MeV), the survival probability against neutron emission of the single-neutron removal residues from $N = 84$ projectiles becomes rather small. Conversely, $N = 82$ remnants produced
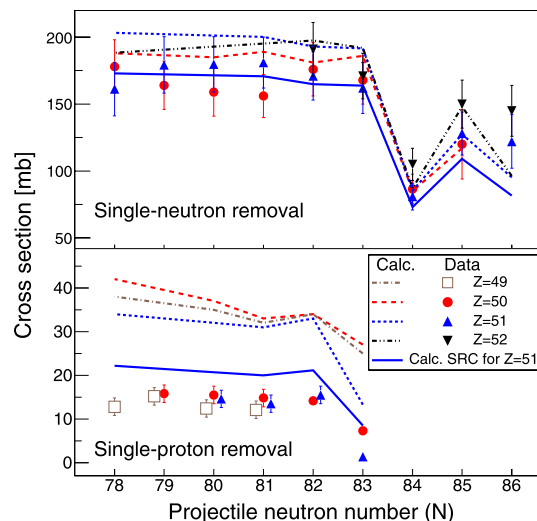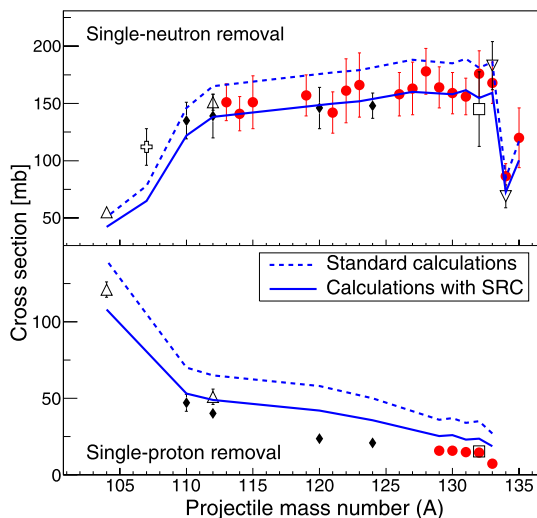

Fig. 3. Single-neutron (upper panel) and single-proton removal cross sections obtained for different isotopes of indium, tin, antimony, and tellurium. Lines represent standard model predictions (dashed and dotted lines) and predictions including a phenomenological description of the impact of SRC nucleon pairs (solid line).

in the single-neutron removal of $N = 83$ projectiles do not populate orbitals above the $N = 82$ shell gap and the populated hole states are close to the Fermi level. The excitation energy gained in that case is rather small, while the binding energy is relatively large (e.g. $S_n(^{132}$Sn$)=7.2$ MeV). The survival probability of the remnants produced in the single-neutron removal of $N = 83$ isotopes is therefore rather high. This argument is also valid for all $N < 84$ projectile nuclei. The increase of the cross section for $N = 85$ can also be explained by the large binding energies compared to the excitation energies of the populated states.

Single-proton removal cross sections, shown in the lower panel in Fig. 3, are also very similar for all isotones until $N = 83$ where they drop. Moreover, the cross section for ^{133}Sn is slightly higher than for ^{134}Sb. This behavior can also be explained by using arguments similar to those discussed above for the single-neutron removal. The decrease in cross section at $N = 83$ is due to the lower survival probability of those remnants against neutron emission because of the low binding energies. Moreover, the larger excitation energy expected by the removal of a proton in nuclei with occupied orbitals above the $Z = 50$ shell reduces the survival probability of ^{134}Sb with respect to ^{133}Sn. Below $N = 83$ the effect of the larger excitation energies in $Z > 50$ remnants does not seem to be sufficient to overcome the larger neutron binding energies.

Another remarkable fact is, that single-proton removal cross sections are about an order of magnitude smaller than those for single-neutron removal. This difference has also been observed in nucleon-removal cross sections obtained with stable medium-mass and heavy nuclei (e.g. ^{112,124}Sn [23], ^{136}Xe [24], ^{197}Au [25], ^{208}Pb [26], and ^{238}U [27]), and with a few unstable medium-mass nuclei (e.g. ^{132}Sn [28], ^{90}Sr [29], ^{137}Cs [29]). The common feature to all these measurements is that they concern neutron-rich nuclei. One could then expect that the mentioned difference in cross sections is caused by the larger excess of neutrons at the nuclear surface. However, previous works, taking into account realistic radial distributions of protons and neutrons in some of these nuclei, could not account for the observed differences in cross section [23].

In Fig. 4 we depict the single-neutron (upper panel) and single-proton (lower panel) removal cross sections measured in this work for different tin isotopes (dots) together with similar measurements reported in literature: ^{133,134}Sn [30] (inverted triangles), ^{132}Sn [28] (square), ^{124,120,112,110}Sn [23] (rhomboids), ^{112,104}Sn [31] (triangles), and ^{107}Sn [32] (cross). The good agreement be-

Fig. 4. Single-neutron (upper panel) and single-proton (lower panel) removal cross sections for different tin isotopes measured in this work (dots) and by other authors. Lines represent standard model predictions (dashed lines) and predictions including a phenomenological description of the impact of SRC nucleon pairs (solid line).

Fig. 5. Upper panel: $0pxn$ removal cross sections for ^{133}Sn and ^{134}Sn compared to previous measurements from Ref. [30]. Lower panel: $1pxn$ removal cross sections for ^{132}Sn. Lines represent standard model predictions (dashed lines) and predictions including a phenomenological description of the impact of SRC nucleon pairs (solid line).

tween coincident measurements validates the results obtained in the present work. Moreover, with the complete set of existing data we systematically cover the single-neutron and single-proton removal cross sections for a large fraction of tin isotopes between ^{104}Sn and ^{134}Sn.

3. Model calculations

Modeling of inclusive nucleon-removal reactions requires the description of all processes leading to a final A-1 residual nucleus. This includes the direct knock-out of a single nucleon, producing a final residue in a bound state, but also initial- and final-state interactions that may contribute to nuclear excitations feeding the A-1 channel, or to the production of A-1 unbound remnants. In particular, inelastic electromagnetic and nuclear excitations, or re-scattering of the knock-out nucleons have to be considered. Moreover, one needs an accurate description of the structure of the involved nuclei, such as their radial distributions of protons and neutrons, and the corresponding single-particle states, as well as spectroscopic factors describing their ground states.

Since a complete theory to describe all the above processes is missing, one should try at least to employ models describing reaction and then structural properties of the involved nuclei in a consistent way. Because of the additional complexity to describe initial- and final state interactions, we decided to use the advanced Liège intra-nuclear cascade (INCL) model providing an accurate description of the knock-out processes, including realistic radial profiles for protons and neutrons [33]. Moreover, this formalism provides a good description of final-state interactions of the knocked-out nucleons, as well as nucleon excitations present in the energy range relevant for this work.

Particle-hole excitations in the remnants were computed using experimental information, if available, and realistic shell model calculations providing the energies and occupations of single-particle orbitals. These calculations were done using a ^{88}Sr core with the orbitals $1p_{1/2}$, $0g_{9/2}$, $0g_{7/2}$, and $1d_{5/2}$ as model space for protons, and $0g_{7/2}$, $1d_{5/2}$, $1d_{3/2}$, $2s_{1/2}$, and $0h_{11/2}$ for neutrons [34,35]. Hole states were randomly defined considering the occupation of the different valence orbitals and the overlap between the corresponding wave functions and the range of impact parameters for knock-out processes provided by the INCL model.
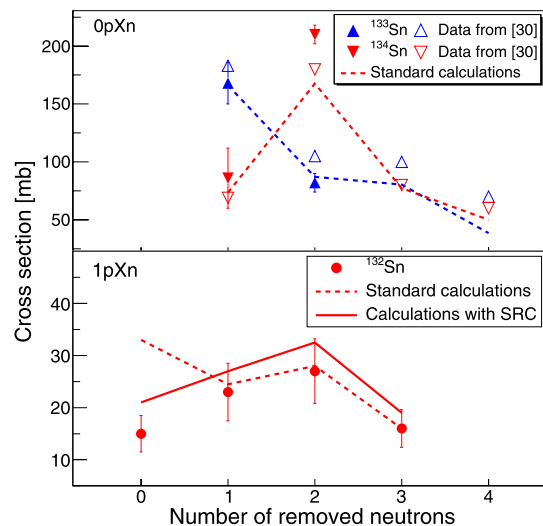
The final excitation of the knock-out remnants was obtained by adding particle-hole excitations and the energy gained in the re-scattering of the outgoing nucleons, as computed by the intra-nuclear cascade model. The survival probability of these remnants was computed as the fraction of the excitation function below the particle emission threshold.

Cross sections and energy gained by electromagnetic and nuclear excitations due to the isovector giant-dipole and the isoscalar giant-quadrupole resonances of the projectile nuclei were computed according to Ref. [36,37]. Here, the fraction of the excitation function between the one- and two-nucleon emission thresholds was accounted as part of the single nucleon-removal cross section. Because most of the investigated nuclei are neutron-rich, these excitations contribute mostly to the single-neutron removal cross section.

4. Results and discussion

The results of the model calculations are depicted with dashed lines in Figs. 3 and 4. The calculations provide a rather good description of the measured neutron-removal cross sections (see upper panel in Fig. 3), in particular the small difference between isotopic chains and the drop in cross section at $N = 84$, due to the $N = 82$ shell gap, as explained in Sect. 2. For heavier isotones, the model calculations slightly underestimate the measured cross sections. This deviation can be explained by the recently observed gamma decay of unbound states in these nuclei [30], not considered in our calculations. The single-neutron knock-out cross sections of lighter isotopes measured in other works, shown in the upper panel of Fig. 4, are also nicely described.

To further check the calculations, in the upper panel of Fig. 5 we depict the multi-neutron removal cross sections for ^{133}Sn and ^{134}Sn. The opposite behavior observed in the cross section of both nuclei for the one- and two-neutron removal for the two nuclei is explained by the influence of the shell gap in the one-neutron removal for $N = 84$ isotones. Again, the model calculations provide an accurate description of the multi-nucleon removal processes. This result is important because it confirms that the model not only properly describes the excitation energy gained by the knock-out remnants around the nucleon emission thresholds, mostly de-
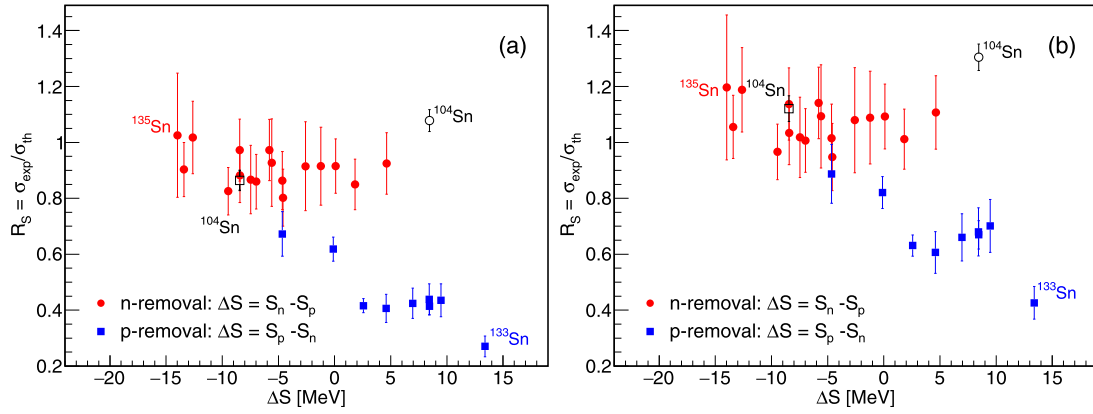
Fig. 6. Ratios of the experimental and calculated inclusive single-nucleon removal cross sections R_s, for a long chain of tin isotopes, as a function of the asymmetry energy ΔS. In the left panel (a), the measured cross sections are normalized to standard model calculations described in Sect. 3. In the right (b) panel the measured values are normalized to model calculation including a phenomenological description of the impact of SRC nucleon pairs in the knock-out process. Solid points correspond to data obtained in the present and our previous work [23], and open points were taken from Ref. [31].

termined by particle-hole excitations, but also the higher excitation energies induced by initial- and final-state interactions.

The surprising result is the large over-prediction of the proton-removal cross sections obtained with the same model calculations, as shown by the dashed lines in the lower panels of Figs. 3 and 4. Moreover, the one-proton x-neutron ($1pxn$) removal cross sections, depicted in the lower panel of Fig. 5, show that this over-prediction mostly affects the single-proton removal channel.

The fact that some 20% of the nucleons inside a nucleus belong to SRC neutron-proton pairs may provide a rather simple explanation [12]. The knock-out of SRC protons induces the emission of the neutron partner, because of their large relative momentum, depopulating the $1p0n$ channel in favor of the $1p1n$. Moreover, in neutron-rich systems the relative fraction of protons in SRC pairs is rather large (i.e. in ^{132}Sn 13 protons and 13 neutrons belong to SRC pairs, representing 26% or the protons and 16% of the neutrons).

The model calculations presented above, were modified to include a phenomenological description of the impact of the SRC neutron-proton pairs in the knock-out process. Every time the INCL model generates the knock-out of a single nucleon in the projectile nucleus, we assume that this nucleon may belong with a certain probability to a nucleon-nucleon pair that breaks, and the two-high momentum nucleons propagate through the nucleus, increasing eventually its excitation energy by further re-scattering, and finally escaping. The probability to knock-out a proton or a neutron from a SRC pair is obtained assuming that 20% of the nucleons belong to neutron-proton pairs. For symmetric nuclei, the fraction of protons and neutrons in SRC pairs will be then 20%. However, along an isotopic chain, as the ones we have investigated, the relative number of neutrons in SRC pairs will slightly decrease with the neutron excess (N/Z), while the relative number of protons will increase, as shown in Ref. [12]. As a consequence, for neutron-rich nuclei the probability to knock-out a proton from a SRC pair will be significantly larger than the probability to knock-out a neutron.

These new calculations, producing a depopulation of the $1p0n$ channel in favor of the $1pxn$ ones, provide a better description of the measured single-proton removal cross sections, as shown by the solid lines in the lower panels of Figs. 3, 4, and 5. The too small increase in the cross section for the $1p1n$, with respect to standard model calculations (lower panel in Fig. 5), is explained by the excitation energy gained in the re-scattering of the two outgoing nucleons, populating then $1p2n$ and $1p3n$ channels. On the other hand, the relatively smaller presence of neutrons in SRC pairs, and the slight decrease of its relative fraction as function of

the neutron excess, only produces a small reduction in the previously calculated single-neutron removal cross sections. This is the reason why the final estimates obtained with the new calculations still provide a good description of the data, as shown by the solid lines in the upper panels in Figs. 3 and 4.

To gain a deeper insight into the interpretation of these results we followed Ref. [17], and in Fig. 6 we depict the ratios R_s between the measured single-nucleon removal cross sections and model predictions presented in Fig. 4 for different tin isotopes. These ratios are shown as function of the asymmetry energy for the different nuclei, $\Delta S = S_n - S_p$ for neutron removal and $\Delta S = S_p - S_n$ for the proton removal, being S_n and S_p the binding energies for neutrons and protons, respectively. In the left panel (Fig. 6(a)), we normalize the measured cross sections to standard model calculations (dashed lines in Fig. 4) while in the right panel (Fig. 6 (b)), we normalize the data to model calculations including a phenomenological description of the role of SRC nucleon pairs in the knock-out process (solid lines in Fig. 4).

As can be seen, the ratio R_s for the single-neutron removal does not show any clear dependence with the asymmetry energy. The inclusion of SRC neutron-proton pairs just moves this ratio up for the single-neutron removal by a factor that varies between 17% and 14% along the tin isotopic chain.

The situation for the single-proton removals is completely different. The ratio R_s obtained with the standard calculations (Fig. 6(a)) shows a clear decrease with the asymmetry energy, similar to the one observed in Ref. [17]. However, this strong dependence of the ratio with the asymmetry energy clearly reduces when SRC nucleon pairs are considered in the calculations (Fig. 6(b)). As previously explained, the dominance of neutron-proton SRC pairs causes the fraction of protons belonging to SRC pairs to increase along the tin isotopic chain from some 22% up to around 31%. This conclusion is particularly valid if one excludes in this analysis the value obtained for ^{133}Sn. The argument is that the single-proton removal cross section of ^{133}Sn is influenced by strong shell effects, as previously discussed.

The remaining 30% over-prediction of the calculated single-proton removal cross sections does not have a simple interpretation. This deviation could be reduced by increasing the total fraction of SRC nucleons. However, for a fraction above 25% we also observed a too strong reduction in the calculated single-neutron removal cross section. Another possibility would be deficiencies in the reaction model, as for example an underestimation in the calculated excitation energies gained by the remnant nuclei due to particle-hole or final-state excitations. However, both explanations

would also produce an underestimation of the calculated single-neutron removal channels.

5. Conclusions

Measurements of the single-neutron and single-proton removal cross sections over long isotopic chains of medium-mass nuclei confirm the systematic reduction of the proton-removal cross sections for neutron-rich nuclei. Similar reductions in these cross sections were previously observed in lighter and heavier nuclei, indicating that this is a general feature. Model calculations describing the knock-out process together with initial- and final-state interactions reproduce the measured neutron-removal cross sections. Proton-removal cross sections are, however, significantly over-predicted by the same calculations. The presence of SRC on nucleon pairs, and more particularly the dominance of neutron-proton pairs, explains to a large extent the observed quenching. The removal of a SRC proton mostly populates the $1pxn$ channels rather than the $1p0n$. This effect is even larger in neutron-rich systems with a larger relative presence of protons in SRC pairs.

Declaration of competing interest

The authors declare that they have no known competing financial interests or personal relationships that could have appeared to influence the work reported in this paper.

Acknowledgements

Appendix A. Supplementary material

Supplementary material related to this article can be found online at https://doi.org/10.1016/j.physletb.2020.135962.

References

[1] L. Lapikas, Quasi-elastic electron scattering off nuclei, Nucl. Phys. A 553 (1993) 297–308, https://doi.org/10.1016/0375-9474(93)90630-G.

[2] J.J. Kelly, Nucleon Knockout by intermediate energy electrons, Adv. Nucl. Phys. 23 (1996) 75–294, https://doi.org/10.1007/0-306-47067-5_2.

[3] W.H. Dickhoff, C. Barbieri, Selfconsistent Green's function method for nuclei and nuclear matter, Prog. Part. Nucl. Phys. 52 (2004) 377–496, https://doi.org/10.1016/j.ppnp.2004.02.038.

[4] S. Paschalis, et al., Nucleon-nucleon correlations and the single-particle strength in atomic nuclei, Phys. Lett. B 800 (2020) 135110, https://doi.org/10.1016/j.physletb.2019.135110.

[5] T. Wakasa, K. Ogata, T. Noro, Proton-induced knockout reactions with polarized and unpolarized beams, Prog. Part. Nucl. Phys. 96 (2017) 32–87, https://doi.org/10.1016/j.ppnp.2017.06.002.

[6] R.A. Niyazov, et al., Two-nucleon momentum distributions measured in ^{3}He(e,e'pp)n, Phys. Rev. Lett. 92 (2004) 052303, https://doi.org/10.1103/PhysRevLett.92.052303.

[7] A. Tang, et al., n-p short-range correlations from (p, 2p+n) measurements, Phys. Rev. Lett. 90 (2003) 042301, https://doi.org/10.1103/PhysRevLett.90.042301.

[8] K.S. Egiyan, et al., Measurement of two- and three-nucleon short-range correlation probabilities in nuclei, Phys. Rev. Lett. 96 (2006) 082501, https://doi.org/10.1103/PhysRevLett.96.082501.

[9] M.M. Sargsian, New properties of the high-momentum distribution of nucleons in asymmetric nuclei, Phys. Rev. C 89 (2014) 034305, https://doi.org/10.1103/PhysRevC.89.034305.

[10] R. Subedi, et al., Probing cold dense nuclear matter, Science 320 (2008) 1476–1478, https://doi.org/10.1126/science.1156675.

[11] O. Hen, et al., Momentum sharing in imbalanced Fermi systems, Science 346 (2014) 614–617, https://doi.org/10.1126/science.1256785.

[12] M. Duer, et al., Jefferson Lab CLAS Collaboration, Probing high-momentum protons and neutrons in neutron-rich nuclei, Nature 560 (2018) 517–621, https://doi.org/10.1038/s41586-018-0400-z.

[13] M. Duer, et al., Jefferson Lab CLAS Collaboration, Direct observation of proton-neutron short-range correlation dominance in heavy nuclei, Phys. Rev. Lett. 122 (2019) 172502, https://doi.org/10.1103/PhysRevLett.122.172502.

[14] T. Kobayashi, et al., Projectile fragmentation of the extremely neutron-rich nucleus 11Li at 0.79 GeV/nucleon, Phys. Rev. Lett. 60 (1988) 2599–2602, https://doi.org/10.1103/PhysRevLett.60.2599.

[15] A. Navin, et al., Spectroscopy of radioactive beams from single-nucleon knock-out reactions: application to the sd shell nuclei ^{25}Al and ^{26,27,28}P, Phys. Rev. Lett. 81 (1998) 5089–5092, https://doi.org/10.1103/PhysRevLett.81.5089.

[16] A. Gade, et al., Reduced occupancy of the deeply bound 0d 5=2 neutron state in ^{32}Ar, Phys. Rev. Lett. 93 (2004) 042501, https://doi.org/10.1103/PhysRevLett.93.042501.

[17] J.A. Tostevin, A. Gade, Systematics of intermediate-energy single-nucleon removal cross sections, Phys. Rev. C 90 (2014) 057602, https://doi.org/10.1103/PhysRevC.90.057602.

[18] F. Flavigny, et al., Limited asymmetry dependence of correlations from single nucleon transfer, Phys. Rev. Lett. 110 (2013) 122503, https://doi.org/10.1103/PhysRevLett.110.122503.

[19] L. Atar, et al., Quasifree (p, 2p) reactions on oxygen isotopes: observation of isospin independence of the reduced single-particle strength, Phys. Rev. Lett. 120 (2018) 052501, https://doi.org/10.1103/PhysRevLett.120.052501.

[20] M. Gómez-Ramos, A.M. Moro, Binding-energy independence of reduced spectroscopic strengths derived from (p, 2p) and (p,pn) reactions with nitrogen and oxygen isotopes, Phys. Lett. B 785 (2018) 511–516, https://doi.org/10.1016/j.physletb.2018.08.058.

[21] H. Geissel, et al., The GSI projectile fragment separator (FRS): a versatile magnetic system for relativistic heavy ions, Nucl. Instrum. Methods B 70 (1992) 286–297, https://doi.org/10.1016/0168-583X(92)95944-M.

[22] J. Alcántara-Núñez, et al., Isotopic yields of spallation residues produced in 136Xe-induced reactions on deuterium at 500A MeV, Phys. Rev. C 92 (2015) 024607, https://doi.org/10.1103/PhysRevC.92.024607.

[23] J.L. Rodríguez-Sánchez, et al., Knockout and fragmentation reactions using a broad range of tin isotopes, Phys. Rev. C 96 (2017) 034303, https://doi.org/10.1103/PhysRevC.96.034303.

[24] J. Benlliure, et al., Production of medium-mass neutron-rich nuclei in reactions induced by ^{136}Xe projectiles at 1A GeV on a beryllium target, Phys. Rev. C 78 (2008) 054605, https://doi.org/10.1103/PhysRevC.78.054605.

[25] F. Rejmund, et al., Measurement of isotopic cross sections of spallation residues in 800A MeV ^{197}Au + p collisions, Nucl. Phys. A 683 (2001) 540–565, https://doi.org/10.1016/S0375-9474(00)00468-1.

[26] L. Audouin, et al., Evaporation residues produced in spallation of ^{208}Pb by protons at 500A MeV, Nucl. Phys. A 768 (2006) 1–21, https://doi.org/10.1016/j.nuclphysa.2006.01.006.

[27] J. Taieb, et al., Evaporation residues produced in the spallation reaction ^{238}U + p at 1A GeV, Nucl. Phys. A 724 (2003) 413–430, https://doi.org/10.1016/S0375-9474(03)01517-3.

[28] D. Pérez-Loureiro, et al., Production of neutron-rich nuclei in fragmentation reactions of 132Sn projectiles at relativistic energies, Phys. Lett. B 703 (2011) 552–556, https://doi.org/10.1016/j.physletb.2011.08.037.

[29] H. Wang, et al., Spallation reaction study for fission products in nuclear waste: cross section measurements for ^{137}Cs and ^{90}Sr on proton and deuteron, Phys. Lett. B 754 (2016) 104–108, https://doi.org/10.1016/j.physletb.2015.12.078.

[30] V. Vaquero, et al., Gamma decay of unbound neutron-hole states in 133Sn, Phys. Rev. Lett. 118 (2017) 202502, https://doi.org/10.1103/PhysRevLett.118.202502.

[31] L. Audirac, et al., Evaporation-cost dependence in heavy-ion fragmentation, Phys. Rev. C 88 (2013) 041602(R), https://doi.org/10.1103/PhysRevC.88.041602.

[32] G. Cerizza, et al., Structure of ^{107}Sn studied through single-neutron knockout reactions, Phys. Rev. C 93 (2016) 021601(R), https://doi.org/10.1103/PhysRevC.93.021601.

[33] J.L. Rodríguez-Sánchez, et al., Improvement of one-nucleon removal and total reaction cross sections in the Liège intranuclear-cascade model using Hartree-Fock-Bogoliubov calculations, Phys. Rev. C 96 (2017) 054602, https://doi.org/10.1103/PhysRevC.96.054602.

[34] L. Coraggio, A. Gargano, N. Itaco, Double-step truncation procedure for large-scale shell-model calculations, Phys. Rev. C 93 (2016) 064328, https://doi.org/10.1103/PhysRevC.93.064328.

[35] A. Gargano, L. Coraggio, N. Itaco, Effectively-truncated large-scale shell-model calculations and nuclei around ^{100}Sn, Phys. Scr. 92 (2017) 094003, https://doi.org/10.1088/1402-4896/aa7d6d.

[36] C.A. Bertulani, C.M. Campbell, T. Glasmacher, A computer program for nuclear scattering at intermediate and high energies, Comput. Phys. Commun. 152 (2003) 317–340, https://doi.org/10.1016/S0010-4655(02)00824-X.

[37] C.A. Bertulani, Y. Kucuk, R. Lozeva, Fission of relativistic nuclei with fragment excitation and reorientation, Phys. Rev. Lett. 124 (2020) 132301, https://doi.org/10.1103/PhysRevLett.124.132301.